ACS APPLIED MATERIALS & INTERFACES

Research Article

www.acsami.org

Osteogenesis Catalyzed by Titanium-Supported Silver Nanoparticles

Huiliang Cao,[*,†,∥] Wenjie Zhang,[‡,∥] Fanhao Meng,[†] Jinshu Guo,[†] Donghui Wang,[†] Shi Qian,[†] Xinquan Jiang,[*,‡] Xuanyong Liu,[*,†] and Paul K. Chu[§]

[†]State Key Laboratory of High Performance Ceramics and Superfine Microstructure, Shanghai Institute of Ceramics, Chinese Academy of Sciences, Shanghai 200050, China

[‡]Department of Prosthodontics, School of Medicine, Ninth People's Hospital Affiliated to Shanghai Jiao Tong University, 639 Zhizaoju Road, Shanghai 200011, China

[§]Department of Physics and Materials Science, City University of Hong Kong, Tat Chee Avenue, Kowloon, Hong Kong, China

Supporting Information

ABSTRACT: Silver nanoparticles (Ag NPs) were widely explored for antimicrobial applications, whereas the translation into drugs and implantable antibacterial devices provoked serious concerns about their potential cytotoxicity. Herein, Ag NPs with diameters ranging from 4 to 19 nm were in situ fabricated and immobilized on titanium by using a plasma immersion ion implantation process. The particles have a population-dependent capability in activating the integrin α5 orchestrated MAPK/ERK signal cascade of osteoblast differentiation in rat bone marrow stem cells (BMSCs), and promoting osteointegration of titanium. It was demonstrated that the titanium-supported Ag NPs played an important role in motivating integrin α5 through triggering the galvanic hydrogen evolution reactions, which was found in positive correlation with the distribution density of the immobilized Ag NPs. Since cellular uptake is a key factor determining the cytotoxic performance of Ag NPs, the extracellular effects of immobilized Ag NPs on promoting osteogenesis provided new insights into the safe application of nanomaterials, and into designing and developing renewed antibacterial devices with selective toxicity.

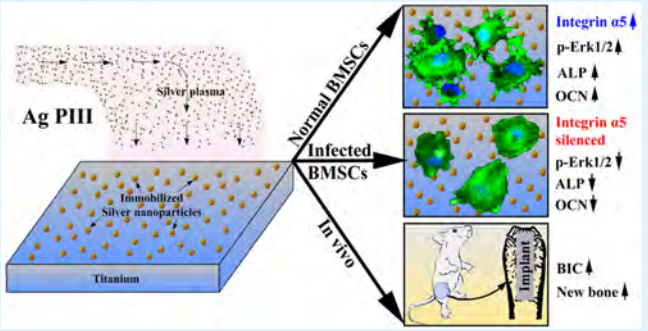

KEYWORDS: *silver, integrin, differentiation, osteointegration, titanium, stem cells*

1. INTRODUCTION

Silver nanoparticles (Ag NPs) were widely explored for antimicrobial applications,[1,2] including implantable antibacterial devices;[3] however, the potential toxicity of the material has raised serious concerns in the biomaterials and biomedical engineering community.[4−6] Evidence from many sources revealed that Ag NPs could be adversaries to various mammalian cells, including embryonic fibroblasts,[7] endotheliocytes,[8] osteoblasts,[9] and mesenchymal stem cells.[10] Cellular uptake is the major pathway that led to the toxic effects of Ag NPs.[4−6] It has revealed a size-dependent toxicity of Ag NPs,[11−13] which demonstrated that the smaller the particles are, the stronger the induced cellular stress is. This was because the small particles (10−20 nm in diameter) entered the cells more easily than the big ones (50−100 nm in diameter).[13] Ag NPs in cells were toxic due to either the whole particles or their dissolution to release of free ionic silver (Ag^+),[14−17] and the latter was fatal because particle dissolution in cytosol was dramatically faster than that in cell culture media.[16,17] Enhancing the intracellular stability of Ag NPs was an effective paradigm to improve their compatibility;[6] nevertheless, it could abolish the antibacterial activity of Ag NPs.[18] Many studies demonstrated that Ag NPs, experimenting with degradable materials, such as calcium phosphate materials[19,20] and polymer,[21] had better experimental outcomes; however, the potential risk of the particles via entering mammalian cells was still there due to the co-releasing manner of these paradigms.

On the other hand, the positive effect of diffusive Ag NPs on osteogenic differentiation of stem cells was also reported in some situations. Qin et al. found that Ag NPs (20 nm) at a low concentration (4 μg/mL) can boost the osteogenic differentiation of human urine-derived stem cells.[22] Also, Zhang et al. demonstrated that Ag NPs with an average diameter of 10 nm promoted the osteogenesis of mesenchymal stem cells at a concentration of 1 mM.[23] These studies suggested that Ag NPs can be selectively toxic, i.e., favoring osteogenesis over bacterial adhesion and biofilm growth, whereas such behavor of purposefully engineered Ag NPs is underexploited. Recently, a proteomic study by Verano-Braga et al. revealed that 100 nm silver particles could extracellularly trigger a cellular response via the serine/threonine protein kinase (PAK), mitogen-activated protein kinase (MAPK), and phosphatase 2A pathways, which did not directly generate reactive oxygen species and damage human colon carcinoma cells.[24] MAPK is

Received: December 1, 2016
Accepted: January 23, 2017
Published: January 23, 2017

DOI: 10.1021/acsami.6b15448
ACS Appl. Mater. Interfaces 2017, 9, 5149−5157

Table 1. Primers for Real-Time Polymerase Chain Reaction (RT-PCR)

gene	prime sequence (F, forward; R, reverse)	product size (bp)	accession no.
ALP	F: GTCCCACAAGAGCCCACAAT	172	NM_013059.1
	R: CAACGGCAGAGCCAGGAAT		
OCN	F: CAGTAAGGTGGTGAATAGACTCCG	172	NM_013414.1
	R: GGTGCCATAGATGCGCTTG		
integrin α5	F: AGAAGACTTTGTTGCTGGCG	173	NM_001108118.1
	R: GCAGGTCATCTAGCCCATCT		
GAPDH	F: GGCAAGTTCAACGGCACAGT	76	NM_017008.3
	R: GCCAGTAGACTCCACGACAT		

involved in the regulation of the osteoblast differentiation of skeletal stem cells,[25] an important process in regeneration of bone tissues. From this view, Ag NPs introduced extracellularly may be a positive stimulus for osteogenesis, which no one has studied yet.

Since the toxicity of nanoparticles is related to the cellular uptake efficiency, we have proposed to study the extracellular actions of Ag NPs by immobilizing them on macroscopic substrates such as titanium plates to reduce the probability of cytophagy. Previously, we have shown that immobilized Ag NPs can act extracellularly against bacteria;[26−29] however, the effects and exact mechanism of Ag NPs on osseointegration of titanium (a commercialized material for implantable medical devices, such as fracture fixation devices, joint prostheses, and dental implants[28]) is unknown. Accordingly, in this study, osteogenic differentiation of rat bone marrow stem cells (BMSCs) on Ag NPs-incorporated titanium is studied on the mRNA level by combination of gene knockout techniques. The results demonstrate that Ag NPs can extracellularly activate the integrin α5 mediated osteogenic cascade of BMSCs to promote osseointegration of titanium.

2. MATERIALS AND METHODS

2.1. Material Preparation and Characterization. *2.1.1. Immobilizing Silver Particles on Titanium.* Polished commercial pure titanium samples (Ti, 10 × 10 mm^2 or 20 × 20 mm^2 square plates with a thickness of 1 mm were used for in vitro studies; 7 mm long cylindrical rods with a diameter of 2 mm were used for in vivo evaluations) were treated by plasma immersion ion implantation by using a filtered cathodic arc of silver (Ag PIII). As a result, silver nanoparticles were in situ precipitated and immobilized on titanium subjected to the atomic-scale heating effect of Ag PIII.[27]

2.1.2. Characterization of the Silver Particles. The morphology and distribution of the silver particles on and underneath titanium surfaces were examined by scanning electron microscopy (SEM) and transmission electron microscopy (TEM). A focused ion beam system was set to thinning the specimens for TEM observations. Dynamic potential polarization curves of the titanium samples before and after immobilization of silver particles were tested in a 0.9% NaCl solution (pH 7). The zeta potential of the sample surfaces was analyzed on an electrokinetic analyzer (Surpass, Anton Parr, Austria) by forcing a sodium chloride (NaCl) electrolyte solution (0.001 M) to flow along the sample surfaces, as detailed before.[28] The electrocatalytic activity of the samples toward the hydrogen evolution reaction (HER) was studied in the phosphate buffer solution (PBS) using linear potential sweep voltammetry (LSV) on a CHI760C instrument (a saturated calomel electrode served as the reference electrode, and a graphite rod was set up to be the counter electrode). Linear sweep voltammetry (LSV) curves were measured by scanning the potential from the corrosion potential down to −2 V at a scan rate of 0.002 V/s. Before polarization, the open circuit potentials were tested for 3600 s to reach a quasistationary state. The silver release manner of the immobilized particles was studied by incubating the 10 × 10 mm^2 square plates in physiological saline (0.9% NaCl solution, 5 mL per each sample) for various periods, and the silver concentration in the resulted solutions was measured by using inductively coupled plasma optical emission spectrometry (ICP-OES).

2.2. In Vitro Responses of BMSCs. *2.2.1. Cell Adhesion.* In order to evaluate the adhesion of the cells, the samples (after seeding the cells on the materials and incubating for 2 h) were rinsed by the phosphate buffered saline solution (PBS, pH7.4) and fixed by a solution of 3% glutaraldehyde (in the sodium cacodylate buffer, pH7.4, Gibco, Invitrogen), followed by permeabilizing in 0.2% Triton X-100 and counterstaining by FITC-Phalloidin (Enzo Life Science Ltd., UK) and DAPI (Sigma), as detailed previously.[28] The morphology of the cell actin and nuclei was imaged with a laser scanning confocal microscopy (LSCM, Leica).

2.2.2. Immunofluorescent Analysis. The immunofluorescent assay was detailed in our previous report.[30] Shortly, after culture in DMEM medium for a desired duration, the samples were fixed by 4% paraformaldehyde, permeabilized by 1% Triton X-100, and blocked by 3% bovine serum albumin. Then, for detection of the alkaline phosphatase (ALP) and osteocalcin (OCN) levels, the cells were treated by the primary antibody against ALP (Abcam) or OCN (Abcam), and counterstained with DyLight 549-conjugated IgG antibody and DAPI (Sigma). To reveal the expression of the integrin α5, the cells were treated sequentially by specific primary antibody targeting integrin α5 (dilution, 1:400; Abcam) and DyLight 549-conjugated antimouse IgG antibody, and the cell cytoskeletons and the nuclei were counterstained with FITC-Phalloidin (Enzo Life Science Ltd., UK) and DAPI (Sigma).

2.2.3. Real-Time Polymerase Chain Reaction. After the cells were cultured for 1, 3, and 7 days, the specimens were rinsed three times with PBS, and the total RNA of the cultured cells was extracted by a TRIZOL reagent (Invitrogen). A 1 mg portion of RNA from each specimen was reverse transcribed into cDNA by a PrimeScript RT reagent kit (TaKaRa) according to the manufacturer's protocols. Real-time polymerase chain reaction (RT-PCR) was performed on a Bio-Rad iQ5 real-time PCR system using a mixture of SYBR Premix Ex TaqII (TaKaRa), cDNA templates, and the primers. ALP, OCN, and integrin α5 of the cultured BMSCs were analyzed with glyceraldehyde-3-phosphate dehydrogenase (GAPDH) serving as an endogenous housekeeping gene for normalization. The primer sequences of the genes were shown in Table 1. Quantification of the gene expressions was based on the comparative cycle-threshold method.

2.2.4. Silencing of Integrin α5 in BMSCs. Three shRNA lentiviral vectors (pGMLV-GFP-shRNA-Intα5, Shanghai Genomeditech Co. Ltd., Shanghai, China) were constructed to silence the expression of integrin α5 in rat BMSCs. They were designed as follows (Table 2): sh-Intα5-1, 5′-gcagatctcggagtcctatta-3′; sh-Intα5-2, 5′-gctatgtca-ctgtccttaatg-3′; sh-Intα5-3, 5′-ggactgaacactaagccttcc-3′. The negative

Table 2. Designed Target Sequence for Silencing Integrin α5 in Rat BMSCs

no.	target sequence
Sh-Intα5-1	GCAGATCTCGGAGTCCTATTA
Sh-Intα5-2	GCTATGTCACTGTCCTTAATG
Sh-Intα5-3	GGACTGAACACTAAGCCTTCC

DOI: 10.1021/acsami.6b15448
ACS Appl. Mater. Interfaces 2017, 9, 5149−5157

control shRNA (sh-NR) species were designed as targeting sequence 5′-ttctccgaacgtgtcacgt-3′. Rat BMSCs were infected with those lentiviruses at a multiplicity of infection (MOI) of 12 in the presence of 8 mg/mL polybrene. Seven days after transfection, the silencing efficiency of different shRNA was determined by RT-PCR. The shRNA with highest silencing efficiency, sh-Intα5-1 was selected for the following experiments. Rat BMSCs infected with sh-NR or sh-Intα5-1 were seeded on different substrates, respectively. After a 7-day culture in DMEM, the total RNA of the cultured cells was extracted by a TRIZOL reagent (Invitrogen). The expression of ALP and OCN was detected using RT-PCR, and glyceraldehyde-3-phosphate dehydrogenase (GAPDH) was served as an endogenous housekeeping gene for normalization.

2.2.5. Western Blot Assay. Western blot assay was carried out to test the expression of Erk1/2 and p-Erk1/2 and reveal the activation of the MAPK/Erk signaling pathways. Briefly, the cells were seeded on the samples and incubated for 12 h. The proteins of the collected cells were extracted according to the manufacturer's instructions of the extraction kit (Biovision). The proteins (20 micrograms) were separated by gel electrophoresis, transferred to nitrocellulose membranes, treated by chemiluminescence reagent (Thermo Fisher Scientific Inc.), and exposed to Kodak X-ray films, as detailed in a previous report.[31] The gray levels of the resulting protein bands were quantified by the Quantity One software (Bio-Rad) and normalized to the β-actin levels. In addition, the immunofluorescent staining of Erk 1/2 and p-Erk 1/2 was also taken to confirm the results of Western blot assay.

2.3. In Vivo Responses of Bone Tissue. *2.3.1. Animals.* The animals for the present study were supplied by the Animal Center of the Ninth People's Hospital (Shanghai, China), and the experimental protocol was authorized by the Animal Care and Experiment Committee affiliated with the Ninth People's Hospital.

2.3.2. Surgical Procedures. According to the surgical protocol previously described,[30] two groups of the samples were randomly implanted in the bilateral femurs of the rats (a total of 12). The two sample groups are (a) commercial pure titanium rods (Ti implant), (b) Ag PIII treated commercial pure titanium rods (Ti-Ag3 implant).

2.3.3. Sequential Fluorescent Labeling. The bone mineralization and integration process around the titanium rods was checked by the fluorescent imaging assay as we described.[32] Briefly, the Alizarin Red S (30 mg/kg, Sigma) and Calcein (20 mg/kg, Sigma) were injected intraperitoneally at the second and the sixth week after the operation, respectively.

2.3.4. Histomorphometric Evaluation. Histomorphometric evaluation was carried out according to the protocols detailed before.[30] Shortly, the bilateral femurs of the animals were harvested at the sixth week after the operations. The randomly selected samples (six per each group) were fixed by 10% buffered formaldehyde, dehydrated by alcohols, embedded in polymethylmetacrylate (PMMA), and cut parallel to the long axis of titanium rods into 150-μm-thick slices and polished for imaging the Alizarin Red S (or Calcein) stained areas. The slices were further stained by van Gieson's picro fuchsin to reveal the bone−implant interfaces. The fluorescent areas, the new bone areas around the interfaces, and bone−implant contact (BIC) rates were quantified by the Image-Pro PlusTM software (Media Cybernetics).

2.4. Statistical Analysis. Statistical analysis was performed by using the SAS 8.2 statistical software package according to the normal distribution and equal variance assumption based one-way ANOVA and SNK posthoc.

3. RESULTS

3.1. Features of the Ag PIII Treated Titanium. The polished titanium (designated as Ti) was smooth on the surface (Figure 1A), while nanoparticles were detected on the substrates (Figure 1B−D) after being treated by silver plasma immersion ion implantation (Ag PIII) at 20 kV for 0.5, 1.0h, and 1.5 h, designated as Ti-Ag1, Ti-Ag2, and Ti-Ag3, respectively. Scanning electron microscopy/energy dispersive X-ray spectroscopy (SEM/EDS) analysis demonstrated that

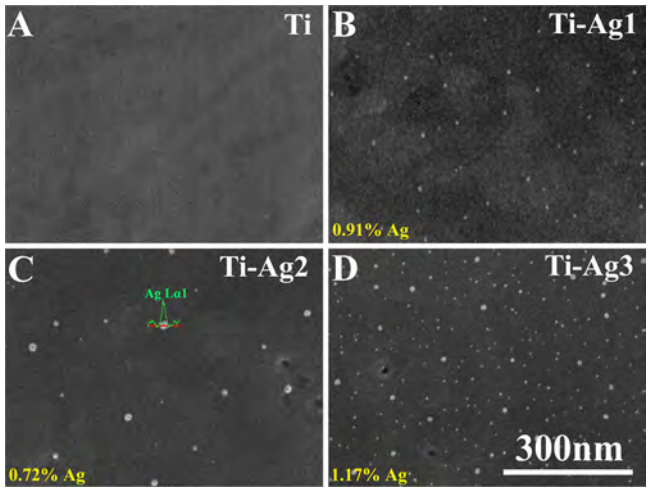

Figure 1. SEM morphology of the polished titanium before and after being treated by silver plasma immersion ion implantation (Ag PIII): (A) the untreated titanium (Ti), (B) the titanium being Ag PIII treated at 20 kV for 0.5 h (Ti-Ag1), (C) the titanium being Ag PIII treated at 20 kV for 1.0 h (Ti-Ag2), and (D) the titanium being Ag PIII treated at 20 kV for 1.5 h (Ti-Ag3). The corresponding XPS-determined silver concentrations are labeled in parts B−D, and a typical SEM/EDS line scan (Ag Lα1) of the nanoparticles is inserted in part C.

these particles were composed of silver (typical line scan was inserted in Figure 1C). The particle diameters for the Ti-Ag1 and Ti-Ag2 groups were in the ranges 4−8 and 4−19 nm, respectively, whereas that for the Ti-Ag3 group can be divided into two subranges, i.e., 4−7 and 9−13 nm. The corresponding particle density (particles per square millimeter) for the Ti-Ag1, Ti-Ag2, and Ti-Ag3 groups was about 1.13×10^8, 0.614×10^8, and 6.56×10^8, respectively. The silver concentration (determined by X-ray photoelectron spectroscopy, XPS) in the surfaces of the Ti-Ag1, Ti-Ag2, and Ti-Ag3 groups was about 0.91%, 0.72%, and 1.17%, respectively. The Ti-Ag3 group was further characterized by transmission electron microscopy (TEM). Typical high-angle annular dark field scanning transmission electron microscopy (HAADF-STEM) image (Figure 2A) and the corresponding energy dispersive X-ray spectroscopy (EDS) mappings (Figure 2, band C) via STEM confirmed that the particles were metallic silver, which precipitated on and underneath the titanium surface within a depth of about 25 nm. The particles, well-resolved by high-resolution transmission electron microscopy (HR-TEM, Figure 2D), and the corresponding fast Fourier transformed patterns (FFT, Figure 2E,F), were face-centered cubic (FCC) crystals with different orientations. In addition, the diameters of the particles underneath the titanium surface were generally smaller than that on the surface, but their distribution density was dramatically increased (Figure 2D).

Due to immobilization of Ag NPs, the electrochemical property of the titanium surface was changed. As shown in Figure S2, the Ag PIII treated groups are more hydrophobic than the titanium control. The surface zeta potential versus pH plots of the titanium before and after immobilization of Ag NPs were acquired in a sodium chloride solution (0.001 M). As presented in Figure 3A, the potentials on all four groups were negative values at pH 7.0 (the pH used in cell culture), but the potential of Ag PIII treated groups was less negative than that of the Ti control, with the Ti-Ag3 group being the least

DOI: 10.1021/acsami.6b15448
ACS Appl. Mater. Interfaces 2017, 9, 5149−5157

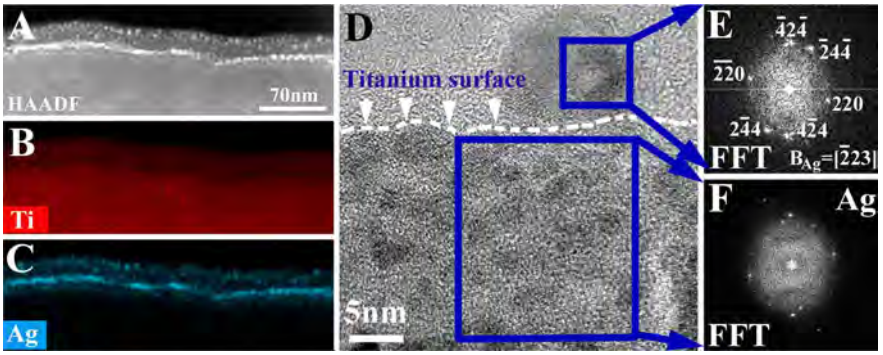

Figure 2. Cross-sectional TEM of the Ti-Ag3 group: (A) the HAADF-STEM image, (B, C) the corresponding EDS mappings of titanium and silver in part A, (D) typical HR-TEM image, (E, F) the corresponding FFT pattern of the circled areas in part D.

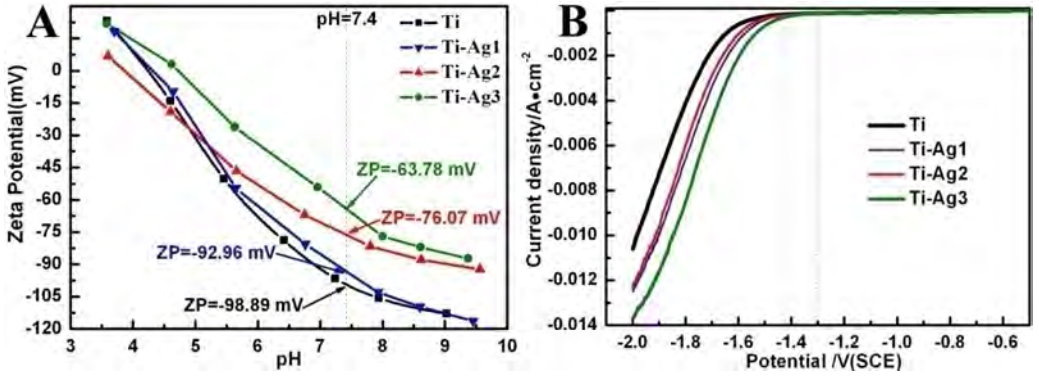

Figure 3. Electrochemical properties of the titanium surface before and after immobilization of Ag NPs: (A) the surface zeta potential versus pH plots, and (B) the linear sweep voltammetry curves.

negative (−63.78 mV) and the Ti-Ag1 group being the most negative (−92.96 mV). Moreover, the electrocatalytic properties of Ag PIII modifiled titanium for the hydrogen evolution reaction (HER) were investigated in PBS solution by means of cathodic polarization. As the linear sweep voltammetry (LSV) curves show in Figure 3B, the proton reduction for the Ag PIII groups starts at a potential that is less negative than that of the bare titanium control. Also, as the particle density in the Ag PIII groups has grown, the corresponding starting potential was shifted toward positive, with the Ti-Ag3 (of the highest particle density among the Ag PIII groups) being the most active group for stimulating HER. In addition, the immobilized particles released a minimal amount of silver. Only ~61 nM of silver was detected in the solution in which a 10 × 10 mm^2 square plate of the Ti-Ag3 group (with the highest silver concentration) incubated for 7 days. Also, this value was not increased while the incubating duration was prolonged to 14 days (measured as ~58 nM).

3.2. Adhesion and Osteoblastic Differentiation of BMSCs. The initial adhesion of rat bone marrow stem cells (BMSCs) was studied by laser scanning confocal microscopy (LSCM) after the cells were cultured on the materials for 2 h and stained with FITC-Phalloidin (green) and DAPI (blue) to visualize their filamentous F-actin and nuclei. As the results show in Figure S1, the rat BMSCs can adhere well on all the groups; however, the cells on the Ag PIII treated groups were expressed for filamentous F-actin (indicated by arrows in Figure S1B−D) at levels apparently higher than that on Ti control (it must be noted that this superiority of Ag PIII groups could fade away as the culture duration becomes longer than 5 h in this study), indicating that the immobilized Ag NPs may faciliate cell adhesion by stimulating some extracellular reactions.

Interestingly, immobilization of Ag NPs on titanium was found to improve the osteoblastic differentiation of rat BMSCs. As demonstrated by the immunofluorescent results (Figure 4), the expression of typical osteogenic markers, such as alkaline phosphates (ALP, Figure 4A) and osteocalcin (OCN, Figure 4B) at day 7 on the Ti-Ag3 group was significantly higher than that on Ti control. As mentioned before, the silver release of the Ag PIII groups was minimal; thus, Ag NPs may affect the BMSCs through extracellular pathways. Since integrin $\alpha 5$ is a key player in propagating osteoblastic signals across the cell membrane,[33−35] the expression of $\alpha 5$ integrin subunit in the BMSCs was further evaluated. As shown in Figure 5, the expression of integrin $\alpha 5$ on Ag PIII groups was increasingly enhanced at the mRNA level during in vitro culture from day 1 to day 7 (Figure 5A, the primers used for real-time polymerase chain reaction were listed in Table 1). Also, the enhanced expression of $\alpha 5$ integrin subunit at the protein level was further confirmed by staining with red fluorescence after a 24-h-incubation (that of the Ti and Ti-Ag3 groups was shown in Figure 5B). These results provided solid evidence that the immobilized particles on titanium were able to prime integrin $\alpha 5$ in BMSCs, and subsequently augment the osteoblastic differentiation of the cells.

In order to confirm that integrin $\alpha 5$ is the key site the immobilized Ag NPs acted on, the rat BMSCs infected with sh-NR (the negative control) or sh-Int$\alpha 5$-1 were seeded on Ti and Ag PIII groups, respectively (sh-Int$\alpha 5$-1 is a shRNA lentiviral vector that is able to silence integrin $\alpha 5$, three vectors were screened, Table 2; this one had the best silencing efficiency in

DOI: 10.1021/acsami.6b15448
ACS Appl. Mater. Interfaces 2017, 9, 5149−5157

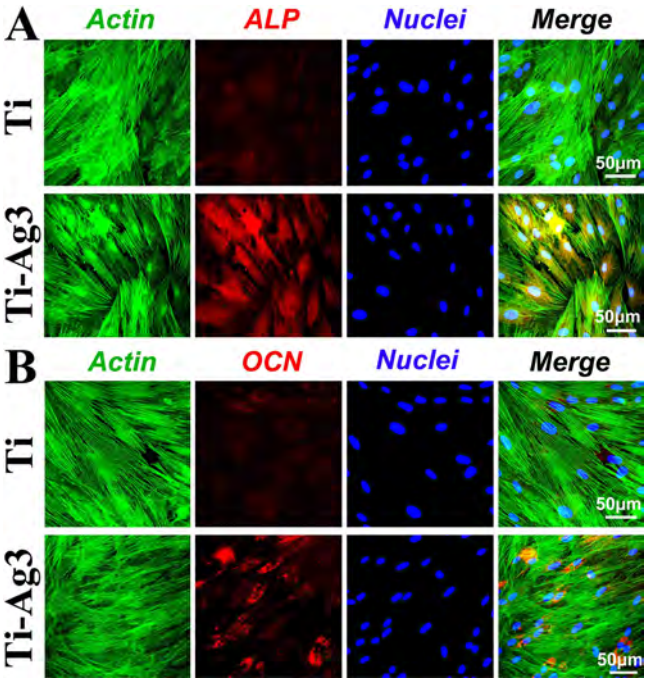

Figure 4. Immunofluorescent staining of typical osteogenic markers in rat BMSCs cultured on Ti and Ti-Ag3 groups for 7 days: (A) alkaline phosphates (ALP), and (B) osteocalcin (OCN).

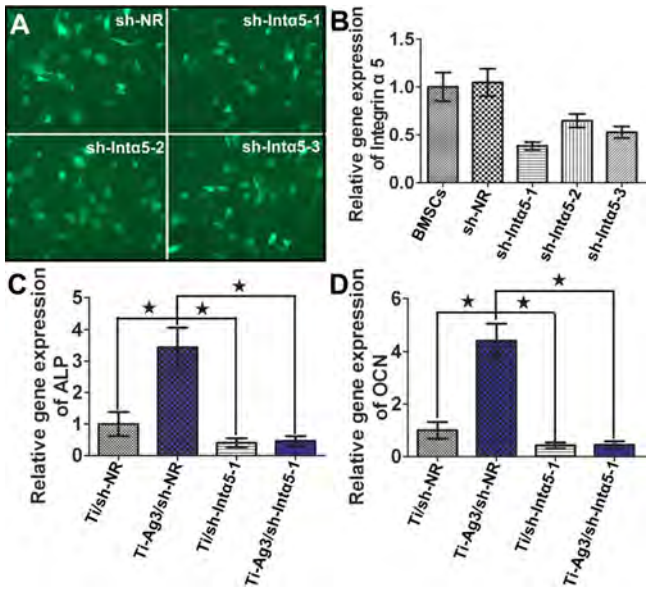

Figure 6. Silencing integrin α5 dismissed the effect of Ag NPs on augmenting osteoblastic differentiation in rat BMSCs: (A) morphology of the rat BMSCs infected with shRNA lentiviral vectors (sh-NR, sh-Intα5-1, sh-Intα5-2, and sh-Intα5-3); (B) silencing efficiency of integrin α5 in rat BMSCs infected with these shRNA lentiviral vectors ("BMSCs" represents the cells were not infected with any vector), evidenced by RT-PCR; (C) the effect of Ag NPs on expression of ALP in rat BMSCs with or without silencing integrin α5, determined by RT-PCR; (D) the effect of Ag NPs on expression of OCN in rat BMSCs with or without silencing integrin α5, determined by RT-PCR. Ti/sh-NR, Ti-Ag3/sh-NR, Ti/sh-Intα5-1, and Ti-Ag3/sh-Intα5-1 represent rat BMSCs infected with sh-NR or sh-Intα5-1 (integrin α5 was silenced), cultured on Ti and Ti-Ag3 groups, respectively. The sh-NR serves as the negative control (integrin α5 was not silenced), and sh-Intα5-1 was used in parts C and D because it had the highest silencing efficiency; ★ represents $p < 0.05$.

rat BMSCs, Figure 6A,B). According to the quantitative RT-PCR results at day 7 (Figure 6C,D), the expression levels of osteogenesis related genes, ALP and OCN in the negative control BMSCs seeded on Ti-Ag3 group, were over three times of that on the Ti control, whereas this superiority of the Ti-Ag3 group over the Ti group was lost after silencing integrin α5. The results strongly indicated that the immobilized Ag NPs enhanced osteogenic differentiation of BMSCs through an integrin α5 mediated pathway. Furthermore, since extracellular signal-regulated kinase 1/2 (ERK1/2) in the mitogen-activated protein kinase (MAPK) family is an important downstream element of the integrin mediated signal transduction machinery controlling the osteogenic differentiation of stem cells,[36] the ERK1/2 and phosphorylated ERK1/2 (p-ERK1/2) levels in the cells were examined by Western blot (WB) and immunostaining assays. The WB results indicated that the Ag PIII treated groups could induce phosphorylation of Erk1/2, and the activation effect of the Ti-Ag3 group was higher than that of the others (Figure 6A,B). Moreover, the effect of Ag NPs on phosphorylation of Erk1/2 was apparently depressed while the integrin α5 in BMSCs was silenced by sh-Intα5-1, as demonstrated by the Ti-Ag3/sh-Intα5-1 group in Figure 6A,B. The result was further supported by the immunostaining assay. As shown in Figure 7C, the phosphorylation of ERK1/2 (p-Erk1/2) in the Ti-Ag3 group was markedly stronger than that in Ti control, whereas the difference was narrowed sharply by silencing integrin α5 with sh-Intα5-1 (the Ti-Ag3/sh-Intα5-1 group in Figure 7C). These results further confirmed that the Ag PIII treated titanium promoted the osteoblastic differ-

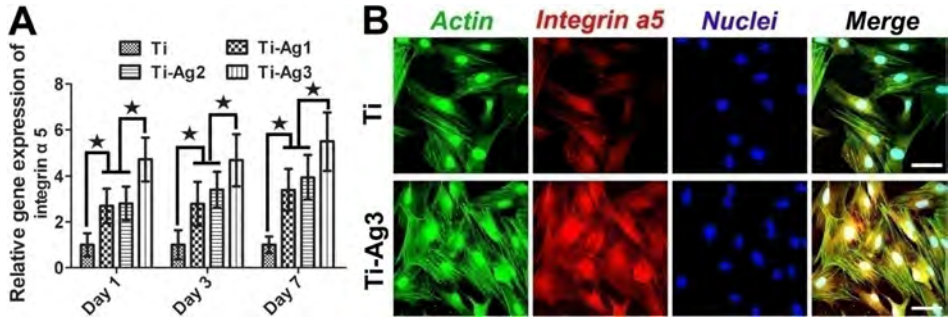

Figure 5. Ag NPs immobilized on titanium were capable of up-regulating the expression of integrin α5 in rat BMSCs, evidenced by (A) real-time polymerase chain reaction (RT-PCR) and (B) immunofluorescent staining of the cells cultured on Ti and Ti-Ag3 groups for 24 h; ★ represents $p < 0.05$.

DOI: 10.1021/acsami.6b15448
ACS Appl. Mater. Interfaces 2017, 9, 5149−5157

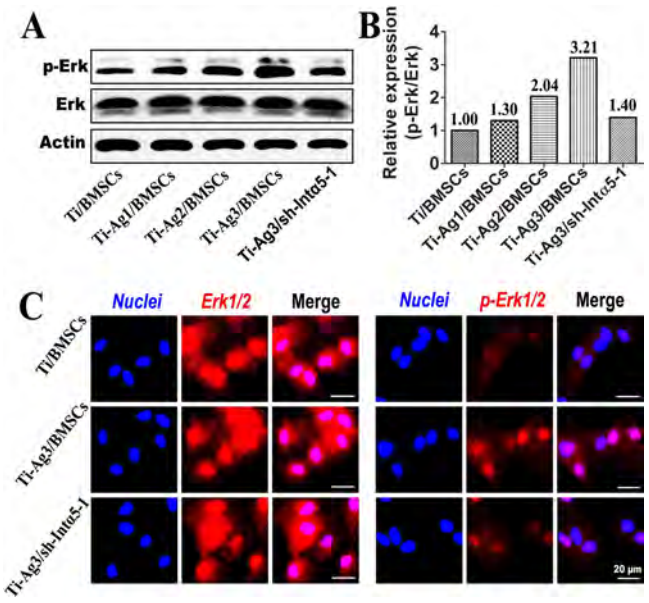

Figure 7. Silencing integrin $\alpha 5$ weakened the effect of Ag NPs on enhancing phosphorylation of extracellular signal-regulated kinase 1/2 (p-ERK1/2) in rat BMSCs: (A, B) Western blot analysis showed the activation of Erk1/2 signaling pathways in BMSCs incubating on various groups for 12 h, and (C) the immunostained Erk1/2 and phosphorylated Erk1/2 (p-Erk1/2) levels in the cells cultured on Ti and Ti-Ag3 groups for 12 h. Ti/BMSCs, Ti-Ag1/BMSCs, Ti-Ag2/BMSCs, and Ti-Ag3/BMSCs represent the normal rat BMSCs cultured on Ti, Ti-Ag1, Ti-Ag2, and Ti-Ag3 groups, respectively. Ti/sh-Intα5-1 represents sh-Intα5-1 infected rat BMSCs cultured on the Ti-Ag3 group.

entiation of BMSCs through overexpression of integrin $\alpha 5$ and then activation of the MAPK/ERK signaling pathway.

3.3. Osteointegration of Ag PIII Treated Titanium. The effect of the immobilized Ag NPs on osteointegration of titanium was evaluated by indwelling cylindrical implants in the femurs of rats and sequential labeling with fluorescent dyes (Figure 8A), and the Ti-Ag3 group was selected for the study because, among the three Ag PIII groups, it presented the strongest effect on stimulating the osteoblastic differentiation of BMSCs in vitro. Alizarin Red S (ARS, red color) was administered at the second week after surgery to reveal the bone formation and mineralization processes around the inserted samples. The results show that the Ti-Ag3 group was almost fully covered by new bone, while those in the Ti group lacked bone integration (ARS in Figure 8B). This trend was consistent with the statistical results (ARS in Figure 8C), which demonstrated that the percentage of the ARS positive area in the Ti-Ag3 group was significantly larger than that in the Ti control. At the sixth week, calcein (green color) was injected into the animals to reveal the subsequent processes of osteointegration. The data demonstrated that the bone around the Ti-Ag3 group grew significantly thicker than that for the Ti group (calcein in Figure 8B), and the trend was confirmed by statistical analysis of the calcein positive area (calcein in Figure 8C). In addition, a large overlapping region (yellow color) was detected around the Ti-Ag3 group (merge in Figure 8B), indicating that meaningful bone remodeling took place in the six week period. The bone−implant interfaces were further detailed by Van Gieson's picro fuchsin staining of the corresponding histological sections. Close apposition of newly formed bone to the Ti-Ag3 group was typically observed (Figure 9A, the Ti-Ag3 implant), while obvious spacing can be spotted between the new bone and the Ti group (Figure 9A, the Ti implant). This trend was backed-up with statistical results, which showed that new bone areas (Figure 9B) and bone−implant contact (BIC) rates (Figure 9C) for the Ti-Ag3 group were significantly higher than that of the Ti control. These results solidly confirmed the positive role of the immobilized Ag NPs on osteointegration of titanium implants.

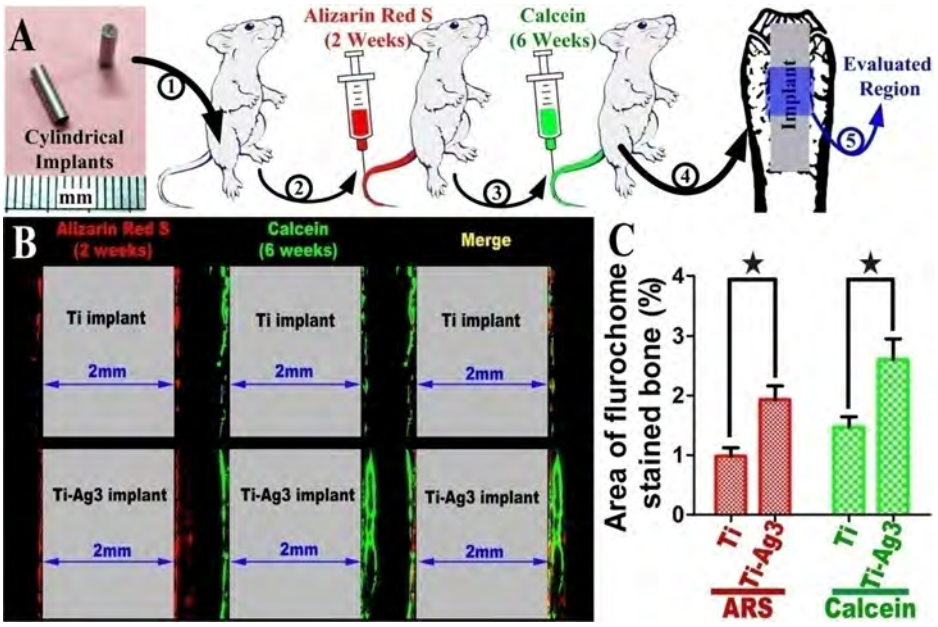

Figure 8. Immobilized Ag NPs accelerated osteointegration of titanium: (A) schematic of surgical procedures, (B) sequential fluorescent labeling the implant-bone boundaries of Ti and Ti−Ag3 groups, (C) percentages of new bone stained with Alizarin Red S (ARS) and calcein in (B); ★ represents $p < 0.05$.

DOI: 10.1021/acsami.6b15448
ACS Appl. Mater. Interfaces 2017, 9, 5149−5157

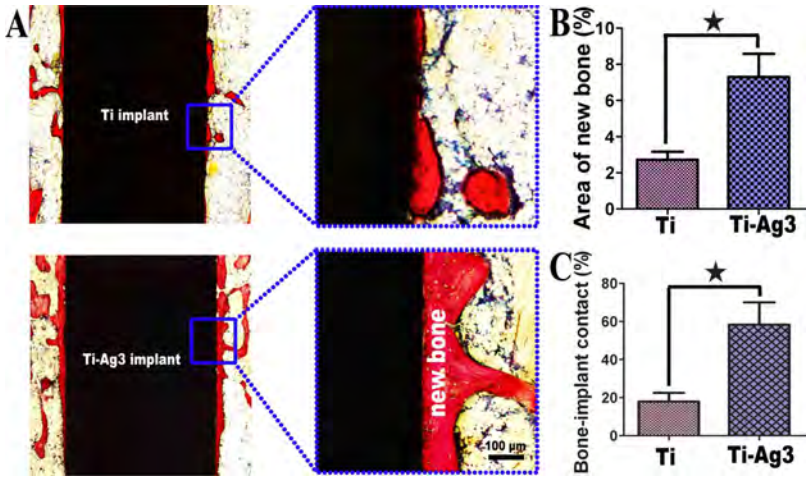

Figure 9. Histological observation and histomorphometric evaluation: (A) After implantation in vivo for 6 weeks, the samples were extracted and prepared into undecalcified sections and further stained with van Gieson's picro fuchsin for histological observation. For the histomorphometric evaluation, (B) the percentage of new bone area around implants and (C) the percentage of bone−implant contact were detected on the low-magnification images.

4. DISCUSSION

Development of tactics that inhibit bacterial colonization as well as promotion of tissue integration was of great significance in the clinic.[37−42] Previously, mobile silver nanoparticles (Ag NPs) were reported to have good antibacterial activity but poison the mitochondrial functions that undermined the apposition of local tissue.[14] Here, it demonstrated that Ag NPs immobilized on titanium extracellularly promoted osteogenic differentiation of BMSCs through priming integrin α5 mediated pathways (Figures 4−6), and significantly promoted the osteointegration of titanium in rats (Figures 7 and 8).

Integrins are transmembrane heterodimeric glycoprotein receptors that propagate bidirectional signals across the plasma membrane;[43] however, they remain in a low-affinity bent state until being activated and transformed into a high-affinity extended conformer with open headpiece,[44] an event that regulates cell fate, directing cells to live or die, to proliferate and differentiate.[43−45] It was evidenced that the headpiece opening of an integrin (an essential step shifts from its equilibrium state toward its high-affinity state) and the establishment and the strength of integrin−ligand interactions are all pH-sensitive.[46,47] For example, the optimum pH varies considerably for different integrin bonds, integrin α2 bound to its physiological ligand within an optimum pH range from pH 7.0 to 8.5,[48] while that for integrin α5 is pH 6.5.[49] On the other hand, the immobilized Ag NPs were found to be capable of promoting the hydrogen evolution reaction (HER) over the titanium support in PBS solution (Figure 3B), and their efficacy in triggering HER was found to positively correlate with particle density. Moreover, since the standard electrode potential of silver (E°_{Ag} = 0.79 V) is more positive than that of titanium (E°_{Ti} = −1.63 V),[50] microgalvanic couples between Ag NPs and the titanium matrix were likely built and could be spontaneously activated in a physiological liquid (this answers for the zeta potential changes over the samples, Figure 3A), encouraging cathodic hydrogen evolution reactions (eqs 1−3) to occur on Ag NPs depending on the oxygen concentraion and the pH value in the solution:[51−54]

$$2H^+ + 2e^- \rightarrow H_2 \ (pH < 7.0) \quad (1)$$

$$2H_2O + 2e^- \rightarrow H_2 + 2OH^- \ (pH \geq 7.0) \quad (2)$$

$$O_2 + 4H^+ + 4e^- \rightarrow 2H_2O \ (pH < 7.0) \quad (3)$$

On account of these reactions, protons (H^+) can be recruited from the adjacent liquid to construct mild acidic local pH gradients between the immobilized particles,[55] which are likely capable of regulating the activities of α5 integrins. As a result, the expression of α5 integrin subunit in the BMSCs was found boosted in the Ag PIII groups (Figure 5), and the Ti-Ag3 group with the highest Ag NPs density (6.56×10^8 particles per square millimeter) and therefore the strongest HER activity (Figure 3) ranked the best among the Ag PIII groups in activating the integrin. In view of this, a possible pathway can be proposed to explain the effects of titanium-supported Ag NPs on augmenting osteogenic differentiation in rat BMSCs and accelerating osteointegration of titanium in vivo (Figure 10): due to the galvanic reactions (eqs 1−3), relative acidic domains were likely formed on Ag PIII treated titanium and facilitated the activation of integrin α5 in BMSCs and the subsequent osteoblastic differentiation as well as bone tissue integration.

In addition, it should be noted that although conformational rearrangements in integrins can be realized via both outside-in and inside-out signaling pathways,[44] the Ag PIII groups can only activate integrin α5 through outside-in pathways, because in the present study, the Ag NPs were immobilized on titanium (Figures 1 and 2) and they released a minimal amount of silver. Since the efficiency in cellular uptake of Ag NPs is a key factor that determines the toxic performance of the material,[4−6] the extracellular effect of titanium-supported Ag NPs on promoting osteogenesis is a highly desired property in developing antibacterial devices with selective toxicity.

5. CONCLUSIONS

Silver nanoparticles (Ag NPs) were in situ precipitated and immobilized on titanium surfaces during the treatment of the plasma immersion ion implantation process. The particles were capable of priming the integrin α5 orchestrated MAPK/ERK signal cascade of osteogenesis in rat BMSCs and effectively accelerating the osteointegration of titanium. This capability was highly related to the density of the Ag NPs, i.e., the more

DOI: 10.1021/acsami.6b15448
ACS Appl. Mater. Interfaces 2017, 9, 5149−5157

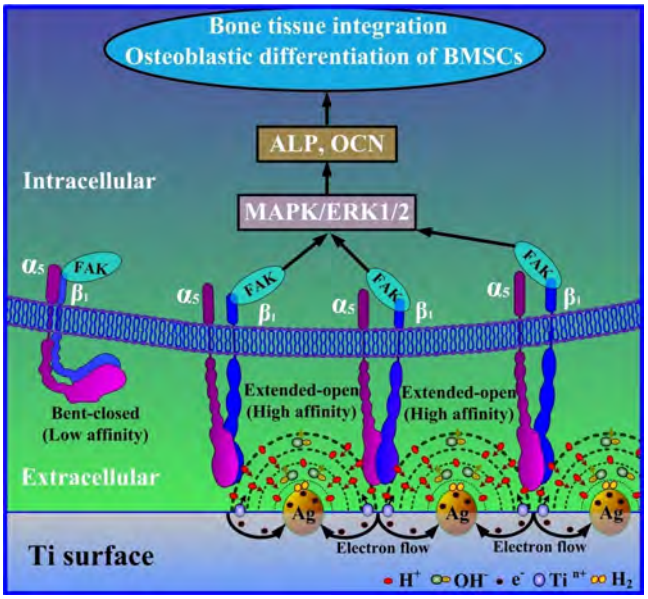

Figure 10. Titanium-supported silver nanoparticle catalyzed the activation of integrin $\alpha5\beta1$, consequently improved the osteoblastic differentiation of rat bone marrow stem cells (BMSCs) in vitro, and enhanced the osteointegration in rats.

particles, the stronger the capacity. It was believed that the titanium-supported Ag NPs played an important role in activating integrin $\alpha5$ through triggering the galvanic hydrogen evolution reactions, which was found in positive correlation with the density of the immobilized particles. This study provided new insights into engineering Ag NPs of selective toxicity for renewed implantable medical devices, which have balanced antibacterial and osteogenic properties.

■ ASSOCIATED CONTENT

Supporting Information

The Supporting Information is available free of charge on the ACS Publications website at DOI: 10.1021/acsami.6b15448.

Initial adhesion of rat bone marrow stem cells (BMSCs) cultured for 2 h on various groups and surface wettability for Ti, Ti-Ag1, Ti-Ag2, and Ti-Ag3 groups (PDF)

■ AUTHOR INFORMATION

Corresponding Authors

*E-mail: hlc@mail.sic.ac.cn.
*E-mail: xinquanj@aliyun.com.
*E-mail: xyliu@mail.sic.ac.cn.

ORCID

Xuanyong Liu: 0000-0001-9440-8143

Author Contributions

‖H.C. and W.Z. contributed equally to this work.

Notes

The authors declare no competing financial interest.

■ ACKNOWLEDGMENTS

This work was jointly supported by the National Science Foundation for Distinguished Young Scholars of China (51525207), National Natural Science Foundation of China (31370962, 31670980, and 81225006), Shanghai Rising-Star Program (15QA1404100), Youth Innovation Promotion Association CAS (2015204), Open Research Fund of State Key Laboratory of Bioelectronics, Southeast University, as well as Hong Kong Research Grants Council (RGC) General Research Funds (GRF) No. City U 11301215. X.J. would like to acknowledge the Chang Jiang Scholars Programme of the Ministry of Education of China.

■ REFERENCES

(1) Eckhardt, S.; Brunetto, P. S.; Gagnon, J.; Priebe, M.; Giese, B.; Fromm, K. M. Nanobio Silver: Its Interactions with Peptides and Bacteria, and Its Uses in Medicine. *Chem. Rev.* **2013**, *113*, 4708−4754.
(2) Chernousova, S.; Epple, M. Silver as Antibacterial Agent: Ion, Nanoparticle, and Metal. *Angew. Chem., Int. Ed.* **2013**, *52*, 1636−1653.
(3) Rizzello, L.; Pompa, P. P. Nanosilver-based Antibacterial Drugs and Devices: Mechanisms, Methodological Drawbacks, and Guidelines. *Chem. Soc. Rev.* **2014**, *43*, 1501−1518.
(4) Nowack, B. Nanosilver Revisited Downstream. *Science* **2010**, *330*, 1054−1055.
(5) Hansen, S. F.; Baun, A. When Enough is Enough. *Nat. Nanotechnol.* **2012**, *7*, 409−411.
(6) Soenen, S. J.; Parak, W. J.; Rejman, J.; Manshian, B. Intra) Cellular Stability of Inorganic Nanoparticles: Effects on Cytotoxicity, Particle Functionality, and Biomedical Applications. *Chem. Rev.* **2015**, *115*, 2109−2135.
(7) Lee, Y. H.; Cheng, F. Y.; Chiu, H. W.; Tsai, J. C.; Fang, C. Y.; Chen, C. W.; Wang, Y. J. Cytotoxicity, Oxidative Stress, Apoptosis and the Autophagic Effects of Silver Nanoparticles in Mouse Embryonic Fibroblasts. *Biomaterials* **2014**, *35*, 4706−4715.
(8) Shi, J.; Sun, X.; Lin, Y.; Zou, X.; Li, Z.; Liao, Y.; Du, M.; Zhang, H. Endothelial Cell Injury and Dysfunction Induced by Silver Nanoparticles Through Oxidative Stress via IKK/NF-κB Pathways. *Biomaterials* **2014**, *35*, 6657−6666.
(9) Albers, C. E.; Hofstetter, W.; Siebenrock, K. A.; Landmann, R.; Klenke, F. M. In Vitro Cytotoxicity of Silver Nanoparticles on Osteoblasts and Osteoclasts at Antibacterial Concentrations. *Nanotoxicology* **2013**, *7*, 30−36.
(10) Hackenberg, S.; Scherzed, A.; Kessler, M.; Hummel, S.; Technau, A.; Froelich, K.; Ginzkey, C.; Koehler, C.; Hagen, R.; Kleinsasser, N. Silver Nanoparticles: Evaluation of DNA Damage, Toxicity and Functional Impairment in Human Mesenchymal Stem Cells. *Toxicol. Lett.* **2011**, *201*, 27−33.
(11) Kim, T. H.; Kim, M.; Park, H. S.; Shin, U. S.; Gong, M. S.; Kim, H. W. Size-dependent Cellular Toxicity of Silver Nanoparticles. *J. Biomed. Mater. Res., Part A* **2012**, *100*, 1033−1043.
(12) Chen, L. Q.; Fang, L.; Ling, J.; Ding, C. Z.; Kang, B.; Huang, C. Z. Nanotoxicity of Silver Nanoparticles to Red Blood Cells: Size Dependent Adsorption, Uptake, and Hemolytic Activity. *Chem. Res. Toxicol.* **2015**, *28*, 501−509.
(13) Verano-Braga, T.; Miethling-Graff, R.; Wojdyla, K.; Rogowska-Wrzesinska, A.; Brewer, J. R.; Erdmann, H.; Kjeldsen, F. Insights Into the Cellular Response Triggered by Silver Nanoparticles Using Quantitative Proteomics. *ACS Nano* **2014**, *8*, 2161−2175.
(14) AshaRani, P. V.; Low Kah Mun, G.; Hande, M. P.; Valiyaveettil, S. Cytotoxicity and Genotoxicity of Silver Nanoparticles in Human Cells. *ACS Nano* **2009**, *3*, 279−2790.
(15) Setyawati, M. I.; Yuan, X.; Xie, J.; Leong, D. T. The Influence of Lysosomal Stability of Silver Nanomaterials on Their Toxicity to Human Cells. *Biomaterials* **2014**, *35*, 6707−6715.
(16) Singh, R. P.; Ramarao, P. Cellular Uptake, Intracellular Trafficking and Cytotoxicity of Silver Nanoparticles. *Toxicol. Lett.* **2012**, *213*, 249−259.
(17) De Matteis, V.; Malvindi, M. A.; Galeone, A.; Brunetti, V.; De Luca, E.; Kote, S.; Kshirsagar, P.; Sabella, S.; Bardi, G.; Pompa, P. P. Negligible Particle-specific Toxicity Mechanism of Silver Nanoparticles: the Role of Ag(+) Ion Release in the Cytosol. *Nanomedicine* **2015**, *11*, 731−739.
(18) Xiu, Z. M.; Zhang, Q. B.; Puppala, H. L.; Colvin, V. L.; Alvarez, P. J. Negligible Particle-specific Antibacterial Activity of Silver Nanoparticles. *Nano Lett.* **2012**, *12*, 4271−4275.

DOI: 10.1021/acsami.6b15448
ACS Appl. Mater. Interfaces 2017, 9, 5149−5157

(19) Lee, J. S.; Murphy, W. L. Functionalizing Calcium Phosphate Biomaterials with Antibacterial Silver Particles. *Adv. Mater.* **2013**, *25*, 1173−1179.
(20) Xie, C. M.; Lu, X.; Wang, K. F.; Meng, F. Z.; Jiang, O.; Zhang, H. P.; Zhi, W.; Fang, L. M. Silver Nanoparticles and Growth Factors Incorporated Hydroxyapatite Coatings on Metallic Implant Surfaces for Enhancement of Osteoinductivity and Antibacterial Properties. *ACS Appl. Mater. Interfaces* **2014**, *6*, 8580−8589.
(21) Lim, Y. H.; Tiemann, K. M.; Heo, G. S.; Wagers, P. O.; Rezenom, Y. H.; Zhang, S.; Zhang, F.; Youngs, W. J.; Hunstad, D. A.; Wooley, K. L. Preparation and In Vitro Antimicrobial Activity of Silver-bearing Degradable Polymeric Nanoparticles of Polyphosphoester-block-poly(L-lactide). *ACS Nano* **2015**, *9*, 1995−2008.
(22) Qin, H.; Zhu, C.; An, Z.; Jiang, Y.; Zhao, Y.; Wang, J.; Liu, X.; Hui, B.; Zhang, X.; Wang, Y. Silver Nanoparticles Promote Osteogenic Differentiation of Human Urine-derived Stem Cells at Noncytotoxic Concentrations. *Int. J. Nanomed.* **2014**, *9*, 2469−2478.
(23) Zhang, R.; Lee, P.; Lui, V. C.; Chen, Y.; Liu, X.; Lok, C. N.; To, M.; Yeung, K. W.; Wong, K. K. Silver Nanoparticles Promote Osteogenesis of Mesenchymal Stem Cells and Improve Bone Fracture Healing in Osteogenesis Mechanism Mouse Model. *Nanomedicine* **2015**, *11*, 1949−1959.
(24) Verano-Braga, T.; Miethling-Graff, R.; Wojdyla, K.; Rogowska-Wrzesinska, A.; Brewer, J. R.; Erdmann, H.; Kjeldsen, F. Insights Into the Cellular Response Triggered by Silver Nanoparticles Using Quantitative Proteomics. *ACS Nano* **2014**, *8*, 2161−2175.
(25) Abdallah, B. M.; Jafari, A.; Zaher, W.; Qiu, W.; Kassem, M. Skeletal Stem Cells: an Update on Intracellular Signaling Pathways Controlling Osteoblast Differentiation. *Bone* **2015**, *70*, 28−36.
(26) Cao, H.; Qiao, Y.; Meng, F.; Liu, X. Spacing-dependent Antimicrobial Efficacy of Immobilized Silver Nanoparticles. *J. Phys. Chem. Lett.* **2014**, *5*, 743−748.
(27) Cao, H.; Qiao, Y.; Liu, X.; Lu, T.; Cui, T.; Meng, F.; Chu, P. K. Electron Storage Mediated Dark Antibacterial Action of Bound Silver Nanoparticles: Smaller is not Always Better. *Acta Biomater.* **2013**, *9*, 5100−5110.
(28) Cao, H.; Liu, X.; Meng, F.; Chu, P. K. Biological Actions of Silver Nanoparticles Embedded in Titanium Controlled by Micro-galvanic Effects. *Biomaterials* **2011**, *32*, 693−705.
(29) Qin, H.; Cao, H.; Zhao, Y.; Jin, G.; Cheng, M.; Wang, J.; Jiang, Y.; An, Z.; Zhang, X.; Liu, X. Antimicrobial and Osteogenic Properties of Silver-ion-implanted Stainless Steel. *ACS Appl. Mater. Interfaces* **2015**, *7*, 10785−10794.
(30) Zhang, W.; Jin, Y.; Qian, S.; Li, J.; Chang, Q.; Ye, D.; Pan, H.; Zhang, M.; Cao, H.; Liu, X.; Jiang, X. Vacuum Extraction Enhances rhPDGF-BB Immobilization on Nanotubes to Improve Implant Osseointegration in Ovariectomized Rats. *Nanomedicine* **2014**, *10*, 1809−1818.
(31) Zhang, W.; Li, Z.; Yan, L.; Ye, D.; Li, J.; Xu, L.; Wei, B.; Zhang, X.; Liu, X.; Jiang, X. Biofunctionalization of a Titanium Surface with a Nano-sawtooth Structure Regulates the Behavior of Rat Bone Marrow Mesenchymal Stem Cells. *Int. J. Nanomed.* **2012**, *7*, 4459−4472.
(32) Zhang, W.; Wang, G.; Liu, Y.; Zhao, X.; Zou, D.; Zhu, C.; Jin, Y.; Huang, Q.; Sun, J.; Liu, X.; Jiang, X.; Zreiqat, H. The Synergistic Effect of Hierarchical Micro/nano-topography and Bioactive ions for Enhanced Osseointegration. *Biomaterials* **2013**, *34*, 3184−3195.
(33) Hamidouche, Z.; Fromigué, O.; Ringe, J.; Häupl, T.; Vaudin, P.; Pagès, J. C.; Srouji, S.; Livne, E.; Marie, P. J. Priming Integrin α5 Promotes Human Mesenchymal Stromal Cell Osteoblast Differentiation and Osteogenesis. *Proc. Natl. Acad. Sci. U. S. A.* **2009**, *106*, 18587−18591.
(34) Fromigué, O.; Brun, J.; Marty, C.; Da Nascimento, S.; Sonnet, P.; Marie, P. J. Peptide-based Activation of α5 Integrin for Promoting Osteogenesis. *J. Cell. Biochem.* **2012**, *113*, 3029−3038.
(35) Srouji, S.; Ben-David, D.; Fromigué, O.; Vaudin, P.; Kuhn, G.; Müller, R.; Livne, E.; Marie, P. J. Lentiviral-mediated Integrin α5 Expression in Human Adult Mesenchymal Stromal Cells Promotes Bone Repair in Mouse Cranial and Long-bone Defects. *Hum. Gene Ther.* **2012**, *23*, 167−172.
(36) Salasznyk, R. M.; Klees, R. F.; Williams, W. A.; Boskey, A.; Plopper, G. E. Focal Adhesion Kinase Signaling Pathways Regulate the Osteogenic Differentiation of Human Mesenchymal Stem Cells. *Exp. Cell Res.* **2007**, *313*, 22−37.
(37) Gristina, A. G. Biomaterial-centered Infection: Microbial Adhesion Versus Tissue Integration. *Science* **1987**, *237*, 1588−1595.
(38) Busscher, H. J.; van der Mei, H. C.; Subbiahdoss, G.; Jutte, P. C.; van den Dungen, J. J.; Zaat, S. A.; Schultz, M. J.; Grainger, D. W. Biomaterial-associated Infection: Locating the Finish Line in the Race for the Surface. *Sci. Transl. Med.* **2012**, *4*, 153rv10.
(39) Raphel, J.; Holodniy, M.; Goodman, S. B.; Heilshorn, S. C. Multifunctional Coatings to Simultaneously Promote Osseointegration and Prevent Infection of Orthopaedic Implants. *Biomaterials* **2016**, *84*, 301.
(40) Li, M.; Liu, X.; Xu, Z.; Yeung, K. W.; Wu, S. Dopamine Modified Organic-Inorganic Hybrid Coating for Antimicrobial and Osteogenesis. *ACS Appl. Mater. Interfaces* **2016**, *8*, 33972−33981.
(41) Xu, Z.; Li, M.; Li, X.; Liu, X.; Ma, F.; Wu, S.; Yeung, K. W.; Han, Y.; Chu, P. K. Antibacterial Activity of Silver Doped Titanate Nanowires on Ti Implants. *ACS Appl. Mater. Interfaces* **2016**, *8*, 16584−16594.
(42) Zhou, T.; Zhu, Y.; Li, X.; Liu, X.; Yeung, K. W. K.; Wu, S.; Wang, X.; Cui, Z.; Yang, X.; Chu, P.K. Surface Functionalization of Biomaterials by Radical Polymerization. *Prog. Mater. Sci.* **2016**, *83*, 191−235.
(43) Giancotti, F. G.; Ruoslahti, E. Integrin Signaling. *Science* **1999**, *285*, 1028−1032.
(44) Takagi, J.; Petre, B. M.; Walz, T.; Springer, T. A. Global Conformational Rearrangements in Integrin Extracellular Domains in Outside-in and Inside-out Signaling. *Cell* **2002**, *110*, 599−611.
(45) Schwartz, M. A.; Ginsberg, M. H. Networks and Crosstalk: Integrin Signalling Spreads. *Nat. Cell Biol.* **2002**, *4*, E65−E68.
(46) Ludwig, F. T.; Schwab, A.; Stock, C. The Na+/H+ Exchanger (NHE1) Generates pH Nanodomains at Focal Adhesions. *J. Cell. Physiol.* **2013**, *228*, 1351−1358.
(47) Paradise, R. K.; Lauffenburger, D. A.; Van Vliet, K. J. Acidic Extracellular pH Promotes Activation of Integrin αvβ3. *PLoS One* **2011**, *6*, e15746.
(48) Eble, J. A.; Tuckwell, D. S. The α2β1 Integrin Inhibitor Rhodocetin Binds to the A-domain of the Integrin α2 Subunit Proximal to the Collagen-binding Site. *Biochem. J.* **2003**, *376*, 77−85.
(49) Lehenkari, P. P.; Horton, M. A. Single Integrin Molecule Adhesion Forces in Intact Cells Measured by Atomic Force Microscopy. *Biochem. Biophys. Res. Commun.* **1999**, *259*, 645−650.
(50) Vanýsek, P. *Electrochemical Series*; CRC Press LLC, 2000.
(51) Carraro, C.; Maboudian, R.; Magagnin, L. Metallization and Nanostructuring of Semiconductor Surfaces by Galvanic Displacement Processes. *Surf. Sci. Rep.* **2007**, *62*, 499−525.
(52) Qian, S.; Zhang, J.; Qu, D. Theoretical and Experimental Study of Microcell and Macrocell Corrosion in Patch Repairs of Concrete Structures. *Cem. Concr. Compos.* **2006**, *28*, 685−695.
(53) Arslan, H.; Celikkan, H.; Ornek, N.; Ersoy, A. E.; Aksu, M. L.; Ozan, O. Galvanic Corrosion of Titanium-based Dental Implant Materials. *J. Appl. Electrochem.* **2008**, *38*, 853−859.
(54) Warkus, J.; Raupach, M.; Gulikers, J. Numerical Modelling of Corrosion-theoretical Backgrounds. *Mater. Corros.* **2006**, *57*, 614−617.
(55) Forslund, M.; Leygraf, C.; Claesson, P. M.; Lin, C.; Pan, J. Micro-galvanic Corrosion Effects on Patterned Copper-Zinc Samples during Exposure in Humidified Air Containing Formic Acid. *J. Electrochem. Soc.* **2013**, *160*, C423−C431.

DOI: 10.1021/acsami.6b15448
ACS Appl. Mater. Interfaces 2017, 9, 5149−5157

Supporting information

Osteogenesis catalyzed by titanium-supported silver nanoparticles

Huiliang Cao *[a,1], *Wenjie Zhang* [b,1], *Fanhao Meng* [a], *Jinshu Guo*[a], *Donghui Wang*[a], *Shi Qian*[a], *Xinquan Jiang**[b], *Xuanyong Liu**[a] , *and Paul K. Chu*[c]

[a]State Key Laboratory of High Performance Ceramics and Superfine Microstructure, Shanghai Institute of Ceramics, Chinese Academy of Sciences, Shanghai 200050, China

[b]Department of Prosthodontics, Ninth People's Hospital Affiliated to Shanghai Jiao Tong University, School of Medicine, 639 Zhizaoju Road, Shanghai 200011, China

[c]Department of Physics and Materials Science, City University of Hong Kong, Tat Chee Avenue, Kowloon, Hong Kong, China

H. Cao-Electronic mail:hlc@mail.sic.ac.cn

X. Jiang-Electronic mail: xinquanj@aliyun.com

X. Liu- Electronic mail: xyliu@mail.sic.ac.cn

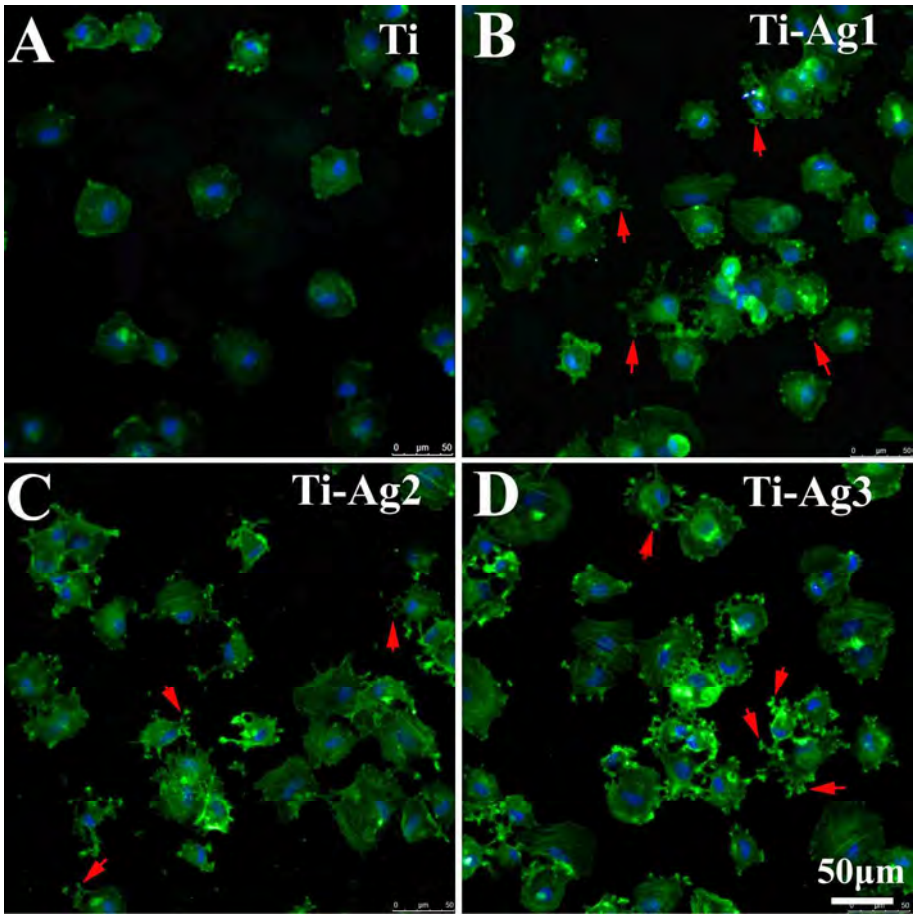

Figure S1. The initial adhesion of rat bone marrow stem cells (BMSCs) cultured for 2 hours on various groups: (A) Ti; (B) Ti-Ag1; (C) Ti-Ag2; (D) Ti-Ag3; The cells were stained with FITC-Phalloidin(Green) and DAPI(Blue) to visualize their filamentous F-actin and nuclei.

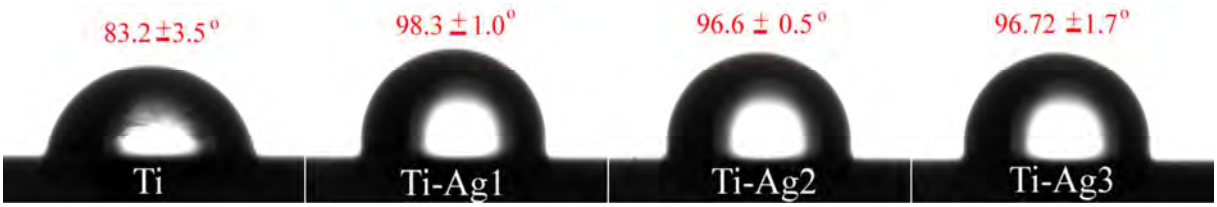

Figure S2. The surface wettability for Ti, Ti-Ag1, Ti-Ag2, and Ti-Ag3 groups; Tested by using one microliter of physiological saline (0.9% NaCl) at room temperature. The Ag PIII treated groups are more hydrophobic than the titanium control (Ti).